Accepted Manuscript

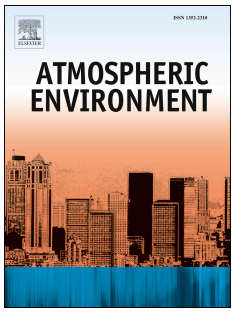

European and Mediterranean mercury modelling: local and long-range contributions to the deposition flux

Christian N. Gencarelli, Francesco De Simone, Ian M. Hedgecock, Francesca Sprovieri, Xin Yang, Nicola Pirrone

PII: S1352-2310(15)30214-4

DOI: 10.1016/j.atmosenv.2015.07.015

Reference: AEA 13951

To appear in: *Atmospheric Environment*

Received Date: 2 April 2015

Revised Date: 7 July 2015

Accepted Date: 10 July 2015

Please cite this article as: Gencarelli, C.N., De Simone, F., Hedgecock, I.M., Sprovieri, F., Yang, X., Pirrone, N., European and Mediterranean mercury modelling: local and long-range contributions to the deposition flux, *Atmospheric Environment* (2015), doi: 10.1016/j.atmosenv.2015.07.015.

European and Mediterranean mercury modelling: local and long-range contributions to the deposition flux

Christian N. Gencarelli[a], Francesco De Simone[a], Ian M. Hedgecock[a], Francesca Sprovieri[a], Xin Yang[b], Nicola Pirrone[c]

[a] *CNR-Institute of Atmospheric Pollution Research, Division of Rende, UNICAL-Polifunzionale, 87036 Rende, Italy*
[b] *British Antarctic Survey, High Cross, Madingley Road, Cambridge,CB3 0ET, United Kingdom*
[c] *CNR-Institute of Atmospheric Pollution Research, Area della Ricerca di Roma 1, Via Salaria km 29,300, Monterotondo, 00015 Rome, Italy*

Abstract

Mercury (Hg) is a global pollutant that is known to have adverse effects on human health, and most human exposure to toxic methylmercury is through fish consumption. Soluble Hg compounds in the marine environment can be methylated in the water column and enter the base of the food chain. Atmospheric deposition is the most important pathway by which Hg enters marine ecosystems. The atmospheric chemistry of Hg has been simulated over Europe and the Mediterranean for the year 2009, using the WRF/Chem model and employing two different gas phase Hg oxidation mechanisms. The contributions to the marine deposition flux from dry deposition, synoptic scale wet deposition and convective wet deposition have been determined. The Hg deposition fluxes resulting from transcontinental transport and local/regional emission sources has been determined using both Br/BrO and O_3/OH atmospheric oxidation mechanisms. The two mechanisms give significantly different annual deposition fluxes (129 Mg and 266 Mg respectively) over the modelling domain. Dry deposition is more significant using the O_3/OH mechanism, while proportionally convective wet deposition is enhanced using the Br/BrO mechanism. The simulations using the Br/BrO oxidation compared best with observed Hg fluxes in precipitation. Local/regional Hg emissions have the most impact within the model domain during the summer. A com-

Email address: ihedegcock@iia.cnr.it (Ian M. Hedgecock)

parison of simulations using the 2005 and 2010 AMAP/UNEP Hg emission inventories show that although there is a decrease of 33% in anthropogenic emissions between the two reference years, the total simulated deposition in the regions diminishes by only 12%. Simulations using the 2010 inventory reproduce observations somewhat better than those using the 2005 inventory for 2009.

Keywords: Mercury, Modelling, Mediterranean, Deposition

1. Introduction

Mercury (Hg) is a global pollutant, and the subject of the recent Minamata convention (`http://www.mercuryconvention.org/`) which aims to protect the environment and human health from the deleterious effects of Hg exposure (Selin, 2014). As was the case in Minamata (see the Minamata mercury events timeline in UNEP (2013b,a))most human exposure to methylmercury is through the consumption of contaminated sea food (Chen et al., 2008; Oken et al., 2012). Methylmercury bioaccumalates through the food web and therefore is found in high concentrations in long-lived piscivorous fish.

Recent research suggests that inorganic Hg compounds can be methylated in the water column (see Sunderland et al. (2009); Mason et al. (2012); Blum et al. (2013); Lamborg et al. (2014); Žagar et al. (2014)). The main input of inorganic Hg (as Hg^{II} compounds) to marine ecosystems occurs via deposition from the atmosphere, through both dry and wet deposition processes. A number of global, regional and box models to study the Hg cycle in the atmosphere have been developed over the last 20 years. Recently with the advent of ever more powerful computers, the possibilities for modelling atmospheric, oceanic, terrestrial and riverine Hg have multiplied. A recent review by Ariya et al. (2015) gives a very thorough summary of recent modelling progress, and stumbling blocks that still exist. Using the WRF/Chem-Hg model simulations of the atmospheric Hg cycle over Europe and the Mediterranean for the year 2009 have been performed using the most recent AMAP/UNEP anthropogenic emission inventory (2010) (AMAP/UNEP, 2013). The results are compared to those obtained using the 2005 emission inventory (AMAP/UNEP, 2008), to see how the differences in the inventories – total emissions, speciation and emission height – impact on the simulated Hg deposition fields. The results have been analysed in order to evaluate the contribution to total Hg deposition fluxes from dry, synoptic and convective wet deposition. The Mediterranean troposphere is influenced by emissions originating within Europe, North America and even Asia (Lelieveld et al., 2002), and therefore model runs with the aim distinguishing the local, versus long-range transport, contributions to the deposition fields were performed. The results using the 2005 and 2010 emission inventories were compared to see how much the reduction of local anthropogenic emissions was reflected in proportion of Hg deposition from local versus long-range transport. Due to the continuing debate over the precise atmospheric Hg oxidation mechanism

(Hynes et al., 2009; Subir et al., 2011, 2012; Weiss-Penzias et al., 2014), simulations using a Br/BrO based Hg oxidation mechanism rather than O_3/OH were performed.

2. Model Description

Gas phase chemistry of Hg and a parametrised representation of atmospheric Hg aqueous chemistry have been added to the RADM2 chemical mechanism in WRF/Chem (version 3.4) using KPP (Sandu and Sander, 2006) and the WKC coupler (Salzmann and Lawrence, 2006). Anthropogenic and natural Hg emissions have also been included and dry and wet deposition processes for Hg have been implemented (see the SI and Gencarelli et al. (2014) for further details).

2.1. Model domain

A coarse domain covering Europe and the Mediterranean, including parts of North Africa and the Middle East (81 by 81 km) and 28 sigma vertical levels from the surface to 50 hPa was used. Within this a nested domain (27 by 27 km) covering all of the Mediterranean and a large part of Europe was used, figure 1. Meteorological input was from the Global Forecast System (GFS, 1°by 1°) at six hourly intervals,and nudging applied for temperature, wind and moisture parameters. Chemical initial and boundary conditions (IC/BC) were taken from the global Hg model ECHMERIT (Jung et al., 2009; De Simone et al., 2014). Further details of the model, and the various physics options employed can be found in Gencarelli et al. (2014) and references therein.

2.2. Emissions

2.2.1. Anthropogenic emissions

Some recent modelling studies have made use of modified anthropogenic emission inventories, either in terms of emission totals or in terms of the emission speciation (see for example Selin et al. (2008); Amos et al. (2012); Kos et al. (2013); Horowitz et al. (2014)). However, these studies mostly consider the problem of Hg speciation in coal fired power plants as specified in the U.S. National Emissions Inventory. The speciation of Hg in the AMAP/UNEP emissions inventory has been questioned (Bieser et al., 2014), however this study referred to the 2005 inventory and not the most recent 2010 inventory. The AMAP/UNEP 2010 inventory (AMAP/UNEP, 2013) is

a significant improvement over the 2005 version (AMAP/UNEP, 2008) and has been used here. However a year long simulation using the 2005 inventory was also performed in order to assess how significant the changes in emissions and deposition are over the modelling domain, and particularly in terms of deposition to the Mediterranean. The differences in the two inventories (for the fine modelling domain used in this study can be found in Table A.1.
For non-mercury anthropogenic emissions the RETRO (`http://www.retro.enes.org/`) and EDGAR v4 (`http://www.edgar.jrc.ec.europa.eu/`) databases were used.
The WRF/Chem emission preprocessor package (Freitas et al., 2011) was used to prepare all the anthropogenic emission input files.

2.2.2. Natural emissions

Hg emissions from biomass burning are included making use of the Hg/CO enhancement ratio (Friedli et al., 2009), the FINNv1 emissions inventory (Wiedinmyer et al., 2011) and the built in plume rise module (Grell et al., 2011). Evasion of Hg^0 from the sea surface (based on Wanninkhof (1992) parametrisation), has also been included for all the marine regions in the modelling domain, (see Gencarelli et al. (2014) for details). Biogenic emissions of non-Hg species are calculated on-line with the Guenther scheme (Guenther et al., 1993, 1994), using the option available in WRF/Chem. Biogenic emissions of Hg are not included.

2.3. Hg oxidation

Gas phase oxidation of $Hg^0_{(g)}$ by O_3 and OH were added to the RADM2 mechanism in WRF/Chem using KPP (Damian et al., 2002; Sandu and Sander, 2006) and the WKC coupler (Salzmann and Lawrence, 2006). As described in Gencarelli et al. (2014) aqueous phase oxidation of $Hg^0_{(aq)}$ is parametrised assuming that O_3, OH and Hg in the aqueous phase are in equilibrium with their respective gas phase concentrations according to Henry's Law.
To perform the simulations using the Br oxidation pathway rather than O_3/OH an approach similar to that described in Holmes et al. (2010) has been used. Oxidation of Hg proceeds firstly by reaction with Br to form unstable diatomic $HgBr^*$ (Donohoue et al., 2006), this can then either react further with OH or Br to form Hg^{II} (Goodsite et al., 2012), or thermally dissociate to leave Hg and Br again.

As in Gencarelli et al. (2014) the oxidation product is assumed to 50:50 soluble Hg^{II} associated with particulate matter and Hg^{II}_g. A fuller description of how soluble and insoluble Hg associated with atmospheric particulate matter can be found in the SI. The oxidation reactions used in the model are shown in table 1.

Reaction	Rate constant cm^3 $molecule^{-1}$ s^{-1}	Reference
(1) $Hg^0 + O_3 \longrightarrow \frac{1}{2}Hg^{II} + \frac{1}{2}Hg^{II}_{(aq)}$	$3.0 \cdot 10^{-20}$	Hall (1995)
(2) $Hg^0 + OH \longrightarrow \frac{1}{2}Hg^{II} + \frac{1}{2}Hg^{II}_{(aq)}$	$8.7 \cdot 10^{-14}$	Sommar et al. (2001)
(3) $Hg^0_{(aq)} + O_{3(aq)} \longrightarrow Hg^{II}_{(aq)}$	$4.7 \cdot 10^{7}$ (*)	Munthe (1992)
(4) $Hg^0 + Br \longrightarrow HgBr$	$3.7 \cdot 10^{-13}$ $(T/298)^{-2.76}$	Goodsite et al. (2012)
(5) $HgBr + Br \longrightarrow \frac{1}{2}Hg^{II} + \frac{1}{2}Hg^{II}_{(aq)}$	$2.5 \cdot 10^{-10}$ $(T/298)^{-0.57}$	Goodsite et al. (2004)
(6) $HgBr + OH \longrightarrow \frac{1}{2}Hg^{II} + \frac{1}{2}Hg^{II}_{(aq)}$	$2.5 \cdot 10^{-10}$ $(T/298)^{-0.57}$	Goodsite et al. (2004)
(4) $HgBr \longrightarrow Hg^0 + Br$	$4.0 \cdot 10^{9}$ exp(-7292/T)	Goodsite et al. (2012)

Table 1: Reactions used in the model. (*) units are M^{-1} s^{-1}.

Br and BrO input concentrations were obtained from the off-line three-dimensional tropospheric chemical transport model p-TOMCAT, modified to include a detailed bromine chemistry scheme (Yang et al., 2005, 2010). The 6 hourly output from p-TOMCAT was interpolated to hourly values using the ratio between incoming solar radiations and daily maximum solar shortwave radiation. The validation of tropospheric bromine chemistry models is hampered by a lack of measurements, most validation is performed by comparing modelled atmospheric column BrO with satellite retrievals hence without vertical resolution, see Parrella et al. (2012).

However, for the marine boundary layer (MBL) the parametrization (based on Platt and Janssen (1995)) used in Holmes et al. (2010) was implemented to calculate hourly Br concentrations,

$$[\mathrm{Br}] = [\mathrm{BrO}]\frac{J_{\mathrm{BrO}} + k_1[\mathrm{NO}]}{k_2[\mathrm{O_3}]} \quad (1)$$

J_{BrO}, [NO] and [O_3] were calculated on-line in the model, k_1 and k_2 were obtained from Platt and Janssen (1995) and a uniform value of 1 ppt was used for [BrO] (Holmes et al., 2010).

2.4. Deposition

Dry deposition of gas phase species in WRF/Chem is treated using the approach developed by Wesely (1989) (see Grell et al. (2005)), and for Hg was calculated as described in Lin et al. (2006). Wet deposition of Hg species has been implemented, adding the Hg compounds to the scheme in WRF/Chem for gas and particulate convective transport and wet deposition. The in-cloud and below-cloud scavenging approach described by Neu and Prather (2012)) has been to adapted to include Hg species. Hg^{II} compounds have been assumed to behave as HNO_3 (Gencarelli et al., 2014), and the original WRF/Chem routine for convective deposition (based on the Grell and Dévényi (2002) parametrization) has been adapted to include the deposition of Hg due to convective precipitation.

2.5. Simulations

The simulations were all performed for the year 2009, and were as follows:

- "Base", complete emission datasets as described in section 2.2, O_3/OH oxidation mechanism, IC/BC from ECHMERIT (De Simone et al., 2014);
- "2005", the same as "Base" but using 2005 anthropogenic emissions, section 2.2.1;
- "Local", as above but without the Hg species BC;
- "Long-range", no emissions within the modelling domain;
- "Br", the same as "Base" but uses the Br oxidation pathway, section 2.3;
- "Br-Local", as "Local" but with Br oxidation;
- "Br-long-range", as "Long-range" but with Br oxidation;

3. Results and Discussion

3.1. Modelled and Observed Hg species concentrations

The simulation results from the "Base", "2005" and "Br" cases have been compared to observations from the European Monitoring and Evaluation Programme (EMEP) monitoring stations (`http://ebas.nilu.no/`), as in Gencarelli et al. (2014). Not all the stations distinguish between $Hg^0_{(g)}$ and $Hg^{II}_{(g)}$ and the modelled values are summed to give Total Gaseous Mercury (TGM) for comparison with observations. Of the EMEP stations within the fine domain during the simulation period, nine measured gas phase Hg,

eight measured Hg associated with particulate matter (Hg^P or PBM), and sixteen collected Hg in precipitation. Only one site (Waldhof, in Germany) had $Hg^{II}_{(g)}$ measurements for 2009, the comparison with model output is included in the SI, these results have also been discussed in Bieser et al. (2014). The frequency of measurements is not the same at all the sites and therefore monthly averaged values of TGM observations have been used (Aas and Breivik, 2011) and the corresponding average calculated from the model output. Comparison of observed and modelled TGM, for all three simulations, are mostly similar to those obtained previously (Gencarelli et al., 2014), although the correlation and bias between observations are slightly improved in the "Base" and "Br" simulations with respect to the "2005" case. The standard deviation in the "Base" case is slightly higher than the "2005" case, but still not as high as the observations, see table A.2.
Whisker and plot figures of the comparison of between the monthly averaged observed and simulated TGM, RGM and PBM, and the monthly total Hg in precipitation are in the SI, figures A.1 - A.4, and the comparison of observed and measured Hg in precipitation can be found in table A.3.
Monthly mean concentrations of PBM are generally well reproduced by the models, while the wet deposition is distinctly overestimated, especially during the spring and summer in the "Base" and "2005" simulations. This suggests that the O_3/OH mechanism tends to produce too much $Hg^{II}_{(g)}$ which is readily scavenged as discussed in Gencarelli et al. (2014).

3.2. The contributions of dry, synoptic scale and convective wet deposition to total deposition flux

The deposition fluxes resulting from dry deposition (DD), synoptic scale wet deposition (SWD) and convective wet deposition (CWD) were summed separately and are reported in table 2 for the "Base", "Br" and "2005" simulations. In all cases it can be seen that DD processes dominate in hot months, with a maximum in July, while wet deposition (WD = SWD + CWD) dominates the Hg deposition flux during the colder months. This tendency is greater in the "Base" and "Br" simulations than it is in the "2005" simulations. The total deposition within the modelling domain, illustrated in 2 is mostly influenced by the oxidation mechanism chosen, and comparing the totals obtained from the "Base" and "2005" runs the difference is $36.9\,\mathrm{Mg\,year^{-1}}$ ($\approx 12\%$). This decrease in deposition depends on a decrease of $73.7\,\mathrm{Mg\,year^{-1}}$ ($\approx 33\%$) in anthropogenic emissions between the two inventories (within the modelling domain), see Table A.1. Therefore over

Europe and the Mediterranean emission reductions have a direct effect on Hg deposition. However, it should also be borne in mind that the characteristics of the anthropogenic emissions differ between the two inventories, in terms of speciation and the emission height distribution.

	Total (Mg)			DD (Mg)			SWD (Mg)			CWD (Mg)		
	Base	2005	Br	Base	2005	Br	Base	2005	Br	Base	2005	Br
Jan	15.6	20.6	12.0	3.6	7.1	4.4	11.7	13.1	6.2	0.4	0.4	1.5
Feb	15.6	19.5	13.6	3.4	6.2	4.0	11.8	13.0	7.9	0.3	0.4	1.7
Mar	21.6	25.0	20.7	5.5	7.5	7.7	15.9	17.2	11.3	0.3	0.3	1.7
Apr	18.4	21.5	12.7	7.6	7.9	5.9	10.4	13.0	6.6	0.4	0.4	0.2
May	21.6	23.2	11.3	10.0	10.3	5.9	10.7	11.9	5.0	1.0	1.0	0.3
Jun	21.4	23.8	8.6	11.0	11.3	5.4	8.9	11.1	2.9	1.4	1.5	0.3
Jul	20.7	22.5	8.3	12.1	12.5	5.9	7.0	8.6	2.1	1.6	1.4	0.3
Aug	43.2	46.4	7.6	21.8	24.5	5.7	18.7	19.3	1.6	2.6	2.6	0.2
Sep	34.4	37.5	8.1	15.9	18.6	5.8	15.9	16.4	2.0	2.6	2.6	0.3
Oct	28.2	31.4	9.2	9.7	12.0	4.9	17.1	18.0	4.1	1.4	1.4	0.3
Nov	14.6	17.7	8.5	5.2	7.4	4.7	9.0	9.9	3.5	0.4	0.4	0.2
Dec	11.0	14.1	8.2	2.7	4.6	3.3	8.0	9.1	4.6	0.3	0.3	0.2
Total	266.3	303.2	128.8	108.5	129.9	63.6	145.1	160.6	57.8	12.7	12.7	7.2
				DD (%)			SWD (%)			CWD (%)		
Jan				22.9	34.3	36.3	74.7	63.7	51.1	2.4	2.0	12.6
Feb				21.8	31.7	29.7	76.0	66.5	57.6	2.1	1.8	12.7
Mar				25.3	30.0	37.3	73.4	68.8	54.8	1.4	1.2	8.0
Apr				41.4	37.1	46.7	56.4	61.1	51.8	2.2	1.8	1.5
May				46.1	44.4	52.8	49.4	51.3	44.5	4.5	4.3	2.7
Jun				51.6	47.5	62.4	41.7	46.4	34.2	6.7	6.1	3.4
Jul				58.4	55.5	70.7	33.7	38.3	25.2	7.9	6.2	4.1
Aug				50.5	52.8	75.7	43.4	41.5	21.7	6.1	5.7	2.6
Sep				46.3	49.5	72.1	46.2	43.6	24.8	7.5	6.9	3.1
Oct				34.3	38.2	53.2	60.7	57.3	43.9	5.0	4.5	2.8
Nov				35.7	41.7	55.5	61.7	56.2	41.6	2.5	2.1	2.9
Dec				24.9	32.8	40.8	72.1	64.8	56.4	3.0	2.4	2.8
Total				40.7	42.8	49.4	54.5	53.0	44.9	4.8	4.2	5.6

Table 2: Monthly Hg deposited by dry deposition (DD), synoptic scale (SWD) and convective (CWD) wet deposition.

The decrease in the deposition flux seen when comparing the "Base" and "2005" simulations is largely due to a decrease in DD over the modelling domain, it decreases by $21.4\,\mathrm{Mg\,year^{-1}}$ ($\approx 12\%$), while SWD decreases by $16.1\,\mathrm{Mg\,year^{-1}}$ ($\approx 10\%$). The decrease in DD is most evident in Autumn and Winter, while the decrease in SWD is more marked in the Spring.
Comparing the "Base" and "Br" simulations the difference in overall depo-

sition flux is immediately apparent. The relative importance of deposition pathways is also different, the "Br" simulation shows a higher proportion of DD and CWD, and relatively lower SWD. The changes in relative deposition flux show that the "Br" case predicts higher relative DD in the summer months and higher wintertime SWD than the "Base" case. The proportion of CWD is higher overall in the "Br" case and particularly so in the early months of the year. The spatial distributions of the deposition fluxes also differ, figures A.5-A.8 show the monthly deposition fluxes of Hg simulated for the "Base" and "Br" cases respectively. Apart from the clear differences in the magnitude of the deposition fluxes predicted by the two simulations, there are significant differences in the spatio-temporal distribution of the fluxes. From figures A.5-A.8 a number of instances of quite different simulated fluxes can be seen. In particular the "Br" simulation predicts high fluxes of CWD in the Eastern Mediterranean in January and February which are not present in the "Base" case. In July, August and September the "Base" simulation predicts high fluxes over most of the Mediterranean Region as well as much of Western/Central Europe, the "Br" case predicts fluxes 4 to 10 times lower. Clearly there is a case to be made for the extension of the current precipitation monitoring network to the south, see figure 1. While it is as yet not possible to experimentally determine DD fluxes with accuracy, the simulations suggest that in a large part of the domain, and particularly in summertime, DD is the dominant deposition pathway. The monthly ratio between wet and dry deposition is shown in figure A.9.

3.3. Local and long-range transport influences on deposition

The centred spatial correlation coefficient (R) between the deposition flux calculated in the "Base" and "Br" simulations and their respective counterparts where only long-range transport or local emissions were considered have been calculated. R is a measure of the correlation between two bidimensional spatial distributions (Santer et al., 1995, 1996), and in the case described here can be used give an indication of the relative influence of long-range Hg transport and local Hg emissions on the simulated deposition flux. Table A.4 shows the monthly spatial correlation coefficients for DD, and WD (SWD+CWD) between the "Base" simulation and the "Local" and "Long-range" simulations, and between the "Br" simulations and the corresponding local and long-range simulations, respectively. Comparing the values of R_{lr}^{DD} and R_{loc}^{DD} it can be seen that DD pattern are mainly affected by long-range Hg transport ($0.62 \leq R_{lr}^{DD} \leq 0.95$). Except in August where

$R_{lr}^{DD} \approx R_{loc}^{DD}$, correlation with DD due to long-range transport is always higher than DD due to local emissions. For WD the influence of long-range transport is principally during the cold months and associated with synoptic scale wet deposition, while stable meteorological conditions, particularly over the Mediterranean Basin during the summer months, result in local emissions having a greater influence on WD fluxes. Long-range transport of Hg is the dominant influence on the Hg deposition flux for a large part of the year (from January to March, and from October to December, with correlation coefficients between 0.60 and 0.90). Local emissions make a greater contribution to Hg deposition in the modelling domain principally in hot months (from April to September with correlation coefficients between 0.70 and 0.82). February shows the largest contribution to WD from long-range transport (0.89), while in September there is the principal contribution to the DD flux (0.98) is from local emissions. Qualitatively the results are in agreement with Lelieveld et al. (2002) in terms of long-range/local influences over the European/Mediterranean region, and with Pongprueksa et al. (2008) in terms of the importance of boundary conditions in determining GEM concentrations and WD flux in a regional scale modelling study (over North America).

4. Discussion

Table 3 sums up the seasonal differences in Hg deposition to land and sea regions in the modelling domain. In the "Br" simulation a third of deposition occurs over the seas, while in the "Base" simulation it is only one quarter. In the "Br" simulation deposition to both the Mediterranean and the Northern European Seas is roughly 35% lower than in the "Base" simulation. Certainly a greater effort to expand the network measuring Hg in precipitation further south is required. The differences seen in the simulated deposition fluxes, and the less obvious differences in TGM and PBM, suggest that the most opportune way to identify Hg impact is to measure deposition rather than gas phase concentrations. However there is no doubt that determining the nature of atmospheric $Hg^{II}_{(g)}$ would be a great step forward in understanding the cycling of Hg in the atmosphere, should be added here. While the case for the Br driven oxidation of $Hg^{0}_{(g)}$ may seem clear, it is not, as it is generally formulated in models up until now, able to explain all the observed variations in atmospheric $Hg^{II}_{(g)}$. A modelling study attempting to reproduce $Hg^{II}_{(g)}$ observations made on board ship during the Mediterranean summer (Sprovieri et al., 2010), showed that the thermal instability of the

		Total		MAM	JJA	SON	DJF
		(Mg)	(%)	(%)	(%)	(%)	(%)
Total	"Base"	266.3		23	32	29	16
	"Br"	128.8		35	20	19	25
Total land	"Base"	200.8	75	23	33	29	15
	"Br"	86.0	67	34	22	21	24
Tot. Marine	"Base"	65.5	25	23	28	31	18
	"Br"	42.8	33	38	17	16	29
Med. Sea	"Base"	34.3	13	22	21	37	21
	"Br"	21.6	17	36	13	14	37
North and	"Base"	9.7	4	20	45	22	11
Baltic Sea	"Br"	6.4	5	42	23	19	17

Table 3: Yearly and seasonal Hg deposited over the different regions of the modelling domain.

$HgBr^*$, 1, means that the Br/BrO mechanism as it is most usually adopted cannot reproduce measured $Hg^{II}_{(g)}$ concentrations in hot weather. The same study also showed that the O_3/OH mechanism greatly overestimated the production of $Hg^{II}_{(g)}$ in the summertime Mediterranean Marine Boundary Layer (MBL). More work is needed to clarify the reactions/mechanisms of atmospheric $Hg^0_{(g)}$ oxidation and also potential atmospheric reduction pathways. The high bias and RMSE seen in the comparison of the simulations using the O_3/OH oxidation mechanism, and the observed Hg in precipitation casts some doubt on the mechanism's ability to reproduce the atmospheric oxidation of Hg. The photoreduction of Hg^{II}-dicarboxylic acid complexes has been suggested as a potential reduction pathway in cloud droplets (Bash et al., 2014). A similar scheme is currently being implemented in WRF/Chem-Hg. It should also be pointed out however that the comparison made here relies on precipitation data from a limited number of sites almost all of which are in the north of Europe and many of which are influenced by westerlies from the Atlantic. It would be extremely useful to have Hg in precipitation measurements from the south of Europe and in the Eastern Mediterranean. One good reason for this is that the higher frequency of convective precipitation in these regions would allow the model to be further constrained, because of the different vertical distributions the O_3/OH and Br/BrO in the troposphere. The Br/BrO mechanism predicts higher free troposphere oxidised

Hg concentrations, and convective precipitation effectively washes out the whole column from the ground to the cloud top. This mechanism therefore simulates higher Hg fluxes than in CWD than does O_3/OH. Conversely the O_3/OH predicts higher oxidised Hg concentrations in the boundary layer, and thus higher Hg deposition from synoptic precipitation. Thus it would be possible to use precipitation data to attempt to distinguish the atmospheric oxidation pathway or pathways.

5. Conclusions

The WRF/Chem-Hg model has been used to evaluate the atmospheric Hg deposition over Europe and the Mediterranean. Anthropogenic and natural emissions, transport and removal processes were simulated for the year 2009 with two different oxidation mechanisms.
The results appear to reinforce the view that the gas phase conversion of $Hg^0_{(g)}$ to $Hg^{II}_{(g)}$ by ozone and the hydroxyl radical is less consistent with observational data and in particular with measured Hg fluxes in precipitation, than the Br/BrO oxidation pathway. Emissions from within the modelling domain correlate most to the overall deposition flux in the summer and long-range transport of Hg contributes most in the winter. Investigating the relative roles of convective and synoptic scale precipitation showed that synoptic scale precipitation is responsible for a far greater deposition flux than convective events. Although the precentage of Hg deposition from CWD is low, it is highest in the "Br" case and most noteiceably so from January to March (table 2). Dry deposition, according to the simulations is a major, and at times the major component of the Hg deposition flux, but at the present time there is no tried and tested experimental way of validating this result. Comparing the simulations performed using the two most recent AMAP/UNEP inventories, 2005 and 2010, showed that the lower emissions in 2010 resulted in lower simulated deposition fluxes, but that the deposition reduction was noticeably less that the emission reduction within the domain.

6. Acknowledgements

We are grateful to the WRF/Chem developers and to the NCAR ESL Atmospheric Chemistry Division for making the WRF/Chem and the WRF/Chem preprocessor codes freely available. We gratefully acknowledge EMEP for

maintaining and making available the database of monitoring station data. The research was performed in the framework of the EU project GMOS (FP7 - 265113) and the National Reference Centre for Mercury (CNRM), Italy. Our thanks to the two anonymous reviewers whose comments helped improve the manuscript.

Aas, W., Breivik, K., 2011. Heavy metals and POP measurements, 2009. Technical Report. Norwegian Institute for Air Research, Kjeller, Norway. EMEP/CCC-Report 3/2011.

AMAP/UNEP, 2008. Technical Background Report to the Global Atmospheric Mercury Assessment. Technical Report. Arctic Monitoring and Assessment Programme, Oslo, Norway / UNEP ChemicalsBranch, Geneva, Switzerland. URL: `http://www.unep.org/hazardoussubstances/Mercury/Informationmaterials/ReportsandPublications/tabid/3593/Default.aspx`.

AMAP/UNEP, 2013. Technical Background Report for the Global Mercury Assessment 2013. Technical Report. Arctic Monitoring and Assessment Programme, Oslo, Norway / UNEP ChemicalsBranch, Geneva, Switzerland. URL: `http://www.unep.org/hazardoussubstances/Mercury/Informationmaterials/ReportsandPublications/tabid/3593/Default.aspx`.

Amos, H.M., Jacob, D.J., Holmes, C.D., Fisher, J.A., Wang, Q., Yantosca, R.M., Corbitt, E.S., Galarneau, E., Rutter, A.P., Gustin, M.S., Steffen, A., Schauer, J.J., Graydon, J.A., Louis, V.L.S., Talbot, R.W., Edgerton, E.S., Zhang, Y., Sunderland, E.M., 2012. Gas-particle partitioning of atmospheric hg(ii) and its effect on global mercury deposition. Atmospheric Chemistry and Physics 12, 591–603.

Ariya, P.A., Amyot, M., Dastoor, A., Deeds, D., Feinberg, A., Kos, G., Poulain, A., Ryjkov, A., Semeniuk, K., Subir, M., Toyota, K., 2015. Mercury physicochemical and biogeochemical transformation in the atmosphere and at atmospheric interfaces: A review and future directions. Chem. Rev. 115, 3760–3802.

Bash, J.O., Carlton, A.G., Hutzell, W.T., Bullock Jr., O.R., 2014. Regional air quality model application of the aqueous-phase photo reduction of atmospheric oxidized mercury by dicarboxylic acids. Atmosphere 5, 1.

Bieser, J., De Simone, F., Gencarelli, C., Geyer, B., Hedgecock, I., Matthias, V., Travnikov, O., Weigelt, A., 2014. A diagnostic evaluation of modeled mercury wet depositions in europe using atmospheric speciated high-resolution observations. Environmental Science and Pollution Research 21, 9995–10012.

Blum, J., Popp, B., Drazen, J., Choy, C., Johnson, M., 2013. Methylmercury production below the mixed layer in the north pacific ocean. Nature Geoscience 6 (10), 879–884.

Chen, C., Amirbahman, A., Fisher, N., Harding, G., Lamborg, C., Nacci, D., Taylor, D., 2008. Methylmercury in marine ecosystems: Spatial patterns and processes of production, bioaccumulation, and biomagnification. EcoHealth 5, 399–408.

Damian, V., Sandu, A., Damian, M., Potra, F., Carmichael, G., 2002. The kinetic preprocessor kpp-a software environment for solving chemical kinetics. Computers and Chemical Engineering 26, 1567–1579.

De Simone, F., Gencarelli, C., Hedgecock, I., Pirrone, N., 2014. Global atmospheric cycle of mercury: a model study on the impact of oxidation mechanisms. Environmental Science and Pollution Research 21, 4110–4123.

Donohoue, D.L., Bauer, D., Cossairt, B., Hynes, A.J., 2006. Temperature and pressure dependent rate coefficients for the reaction of hg with br and the reaction of br with br: A pulsed laser photolysis-pulsed laser induced fluorescence study. The Journal of Physical Chemistry A 110, 6623–6632.

Freitas, S.R., Longo, K.M., Alonso, M.F., Pirre, M., Marecal, V., Grell, G., Stockler, R., Mello, R.F., Sánchez Gácita, M., 2011. Prep-chem-src – 1.0: a preprocessor of trace gas and aerosol emission fields for regional and global atmospheric chemistry models. Geoscientific Model Development 4, 419–433.

Friedli, H., Arellano, A., Cinnirella, S., Pirrone, N., 2009. Initial estimates of mercury emissions to the atmosphere from global biomass burning. Environmental Science & Technology 43, 3507–3513.

Gencarelli, C.N., De Simone, F., Hedgecock, I.M., Sprovieri, F., Pirrone, N., 2014. Development and application of a regional-scale atmospheric

mercury model based on wrf/chem: a mediterranean area investigation. Environmental Science and Pollution Research 21, 4095–4109.

Goodsite, M.E., Plane, J.M.C., Skov, H., 2004. A theoretical study of the oxidation of hg0 to hgbr2 in the troposphere. Environmental Science & Technology 38, 1772–1776.

Goodsite, M.E., Plane, J.M.C., Skov, H., 2012. Correction to a theoretical study of the oxidation of hg0 to hgbr2 in the troposphere. Environmental Science & Technology 46, 5262–5262.

Grell, G., Freitas, S.R., Stuefer, M., Fast, J., 2011. Inclusion of biomass burning in wrf-chem: impact of wildfires on weather forecasts. Atmospheric Chemistry and Physics 11, 5289–5303.

Grell, G.A., Dévényi, D., 2002. A generalized approach to parameterizing convection combining ensemble and data assimilation techniques. Geophys. Res. Lett. 29, 38–1–38–4.

Grell, G.A., Peckham, S.E., Schmitz, R., McKeen, S.A., Frost, G., Skamarock, W.C., Eder, B., 2005. Fully coupled "online" chemistry within the wrf model. Atmospheric Environment 39, 6957–6975.

Guenther, A., Zimmerman, P., Wildermuth, M., 1994. Natural volatile organic compound emission rate estimates for u.s. woodland landscapes. Atmospheric Environment 28, 1197 – 1210.

Guenther, A.B., Zimmerman, P.R., Harley, P.C., Monson, R.K., Fall, R., 1993. Isoprene and monoterpene emission rate variability: Model evaluations and sensitivity analyses. J. Geophys. Res. 98, 12609–12617.

Hall, B., 1995. The gas phase oxidation of elemental mercury by ozone. Water, Air, and Soil Pollution 80, 301–315.

Holmes, C.D., Jacob, D.J., Corbitt, E.S., Mao, J., Yang, X., Talbot, R., Slemr, F., 2010. Global atmospheric model for mercury including oxidation by bromine atoms. Atmospheric Chemistry and Physics 10, 12037 – 12057.

Horowitz, H.M., Jacob, D.J., Amos, H.M., Streets, D.G., Sunderland, E.M., 2014. Historical mercury releases from commercial products: Global environmental implications. Environmental science and technology 48(17), 10242–10250.

Hynes, A.J., Donohoue, D.L., Goodsite, M.E., Hedgecock, I.M., 2009. Our current understanding of major chemical and physical processes affecting mercury dynamics in the atmosphere and at the air-water/terrestrial interfaces, in: Pirrone, N., Mason, R.P. (Eds.), Mercury Fate and Transport in the Global Atmosphere: Emissions, Measurements and Models. Springer. chapter 14, pp. 427–457.

Jung, G., Hedgecock, I., Pirrone, N., 2009. ECHMERIT V1.0 - a new global fully coupled mercury-chemistry and transport model. Geoscientific Model Development Discussions 2, 385–453.

Kos, G., Ryzhkov, A., Dastoor, A., Narayan, J., Steffen, A., Ariya, P.A., Zhang, L., 2013. Evaluation of discrepancy between measured and modelled oxidized mercury species. Atmospheric Chemistry and Physics 13(9), 4839–4863.

Lamborg, C., Bowman, K., Hammerschmidt, C., Gilmour, C., Munson, K., Selin, N., Tseng, C.M., 2014. Mercury in the anthropocene ocean. Oceanography 27(1), 7687.

Lelieveld, J., Berresheim, H., Borrmann, S., Crutzen, P.J., Dentener, F.J., Fischer, H., Feichter, J., Flatau, P.J., Heland, J., Holzinger, R., Korrmann, R., Lawrence, M.G., Levin, Z., Markowicz, K.M., Mihalopoulos, N., Minikin, A., Ramanathan, V., de Reus, M., Roelofs, G.J., Scheeren, H.A., Sciare, J., Schlager, H., Schultz, M., Siegmund, P., Steil, B., Stephanou, E.G., Stier, P., Traub, M., Warneke, C., Williams, J., Ziereis, H., 2002. Global air pollution crossroads over the mediterranean. Science 298, 794–799.

Lin, C.J., Pongprueksa, P., Lindberg, S.E., Pehkonen, S.O., Byun, D., Jang, C., 2006. Scientific uncertainties in atmospheric mercury models i: Model science evaluation. Atmospheric Environment 40, 2911 – 2928.

Mason, R.P., Choi, A.L., Fitzgerald, W.F., Hammerschmidt, C.R., Lamborg, C.H., Soerensen, A.L., Sunderland, E.M., 2012. Mercury biogeochemical cycling in the ocean and policy implications. Environmental Research 119, 101 – 117.

Munthe, J., 1992. The aqueous oxidation of elemental mercury by ozone. Atmospheric Environment. Part A. General Topics 26, 1461 – 1468.

Neu, J.L., Prather, M.J., 2012. Toward a more physical representation of precipitation scavenging in global chemistry models: cloud overlap and ice physics and their impact on tropospheric ozone. Atmospheric Chemistry and Physics 12, 3289–3310.

Oken, E., Choi, A., Karagas, M., Mariën, K., Rheinberger, C., Schoeny, R., Sunderland, E., Korrick, S., 2012. Which fish should i eat? perspectives influencing fish consumption choices. Environ Health Perspect 120, 790–798.

Parrella, J.P., Jacob, D.J., Liang, Q., Zhang, Y., Mickley, L.J., Miller, B., Evans, M.J., Yang, X., Pyle, J.A., Theys, N., Van Roozendael, M., 2012. Tropospheric bromine chemistry: implications for present and pre-industrial ozone and mercury. Atmospheric Chemistry and Physics 12, 6723–6740.

Platt, U., Janssen, C., 1995. Observation and role of the free radicals no3, clo, bro and io in the troposphere. Faraday Discussion 100, 175198.

Pongprueksa, P., Lin, C.J., Lindberg, S.E., Jang, C., Braverman, T., Jr., O.R.B., Ho, T.C., Chu, H.W., 2008. Scientific uncertainties in atmospheric mercury models iii: Boundary and initial conditions, model grid resolution, and Hg(II) reduction mechanism. Atmospheric Environment 42, 1828 – 1845.

Salzmann, M., Lawrence, M.G., 2006. Automatic coding of chemistry solvers in WRF-Chem using KPP, in: 7th WRF Users Workshop, Boulder, Colorado, USA.

Sandu, A., Sander, R., 2006. Technical note: Simulating chemical systems in fortran90 and matlab with the kinetic preprocessor kpp-2.1. Atmospheric Chemistry and Physics 6, 187–195.

Santer, B.D., Taylor, K.E., Wigley, T.M., Penner, J.E., Jones, P.D., Cubasch, U., 1995. Towards the detection and attribution of an anthropogenic effect on climate. Climate Dynamics 12, 77–100.

Santer, B.D., Taylor, K.E., Wigley, T.M.L., Johns, T.C., Jones, P.D., Karoly, D.J., Mitchell, J.F.B., Oort, A.H., Penner, J.E., Ramaswamy, V., Schwarzkopf, M.D., Stouffer, R.J., Tett, S., 1996. A search for human influences on the thermal structure of the atmosphere. Nature 382, 39–46.

Selin, N.E., 2014. Global change and mercury cycling: Challenges for implementing a global mercury treaty. Environmental Toxicology and Chemistry 33, 1202–1210.

Selin, N.E., Jacob, D.J., Yantosca, R.M., Strode, S., Jaeglé, L., Sunderland, E.M., 2008. Global 3-d land-ocean-atmosphere model for mercury: Present-day versus preindustrial cycles and anthropogenic enrichment factors for deposition. Global Biogeochem. Cycles 22, GB2011.

Sommar, J., Gårdfeldt, K., Strömberg, D., Feng, X., 2001. A kinetic study of the gas-phase reaction between the hydroxyl radical and atomic mercury. Atmospheric Environment 35, 3049 – 3054.

Sprovieri, F., Pirrone, N., Ebinghaus, R., Kock, H., Dommergue, A., 2010. A review of worldwide atmospheric mercury measurements. Atmospheric Chemistry and Physics 10, 8245–8265.

Subir, M., Ariya, P.A., Dastoor, A.P., 2011. A review of uncertainties in atmospheric modeling of mercury chemistry I. uncertainties in existing kinetic parameters fundamental limitations and the importance of heterogeneous chemistry. Atmospheric Environment 45, 5664 – 5676.

Subir, M., Ariya, P.A., Dastoor, A.P., 2012. A review of the sources of uncertainties in atmospheric mercury modeling II. mercury surface and heterogeneous chemistry a missing link. Atmospheric Environment 46, 1 – 10.

Sunderland, E.M., Krabbenhoft, D.P., Moreau, J.W., Strode, S.A., Landing, W.M., 2009. Mercury sources, distribution, and bioavailability in the north pacific ocean: Insights from data and models. Global Biogeochem. Cycles 23, GB2010–.

UNEP, 2013a. Mercury: Acting Now! Technical Report. UNEP Chemicals Branch, Geneva, Switzerland.

UNEP, 2013b. Mercury: Time to Act. Technical Report. Chemicals Branch, Division of Technology, Industry and Economics, United Nations Environment Programme.

Wanninkhof, R., 1992. Relationship between wind speed and gas exchange over the ocean. Journal of Geophysical Research: Oceans 97, 7373–7382.

Weiss-Penzias, P., Amos, H.M., Selin, N.E., Sexauer Gustin, M., Jaffe, D.A., Obrist, D.and Sheu, G.R., Giang, A., 2014. Use of a global model to understand speciated atmospheric mercury observations at five high-elevation sites. Atmospheric Chemistry and Physics Discussions 14(16), 22763–22792.

Wesely, M., 1989. Parameterization of surface resistances to gaseous dry deposition in regional-scale numerical models. Atmospheric Environment (1967) 23, 1293 – 1304.

Wiedinmyer, C., Akagi, S.K., Yokelson, R.J., Emmons, L.K., Al-Saadi, J.A., Orlando, J.J., Soja, A.J., 2011. The fire inventory from ncar (finn): a high resolution global model to estimate the emissions from open burning. Geoscientific Model Development 4, 625–641.

Yang, X., Cox, R.A., Warwick, N.J., Pyle, J.A., Carver, G.D., O'Connor, F.M., Savage, N.H., 2005. Tropospheric bromine chemistry and its impacts on ozone: A model study. Journal of Geophysical Research: Atmospheres 110, 19842012.

Yang, X., Pyle, J.A., Cox, R.A., Theys, N., Van Roozendael, M., 2010. Snow-sourced bromine and its implications for polar tropospheric ozone. Atmospheric Chemistry and Physics 10, 7763–7773.

Žagar, D., Sirnik, N., Četina, M., Horvat, M., Kotnik, J., Ogrinc, N., Hedgecock, I.M., Cinnirella, S., De Simone, F., Gencarelli, C.N., Pirrone, N., 2014. Mercury in the Mediterranean. Part 2: processes and mass balance. Environmental Science and Pollution Research 21, 4081–4094.

6.1. Figures

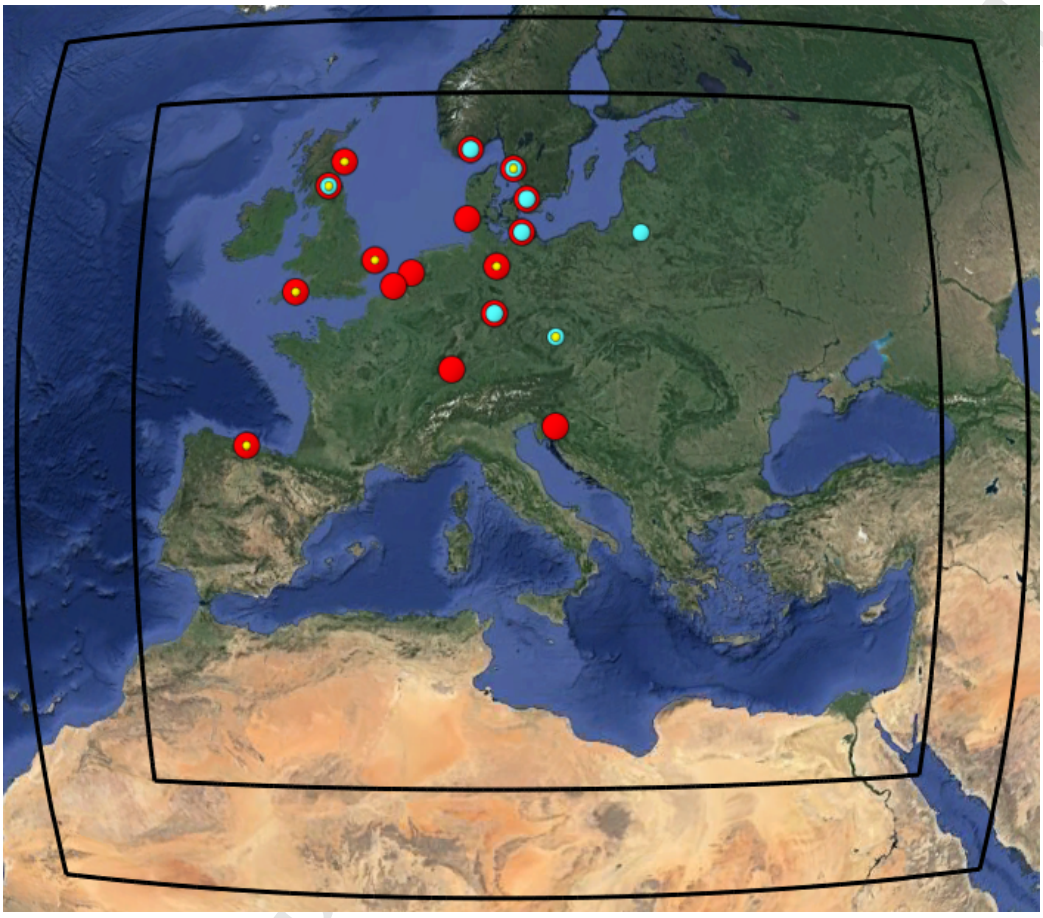

Figure 1: Model domains and location to the EMEP measurement stations used for measurement comparisons (red points for wet deposition, cyan for TGM and yellow for PBM) displayed in Google^{TM} Earth.

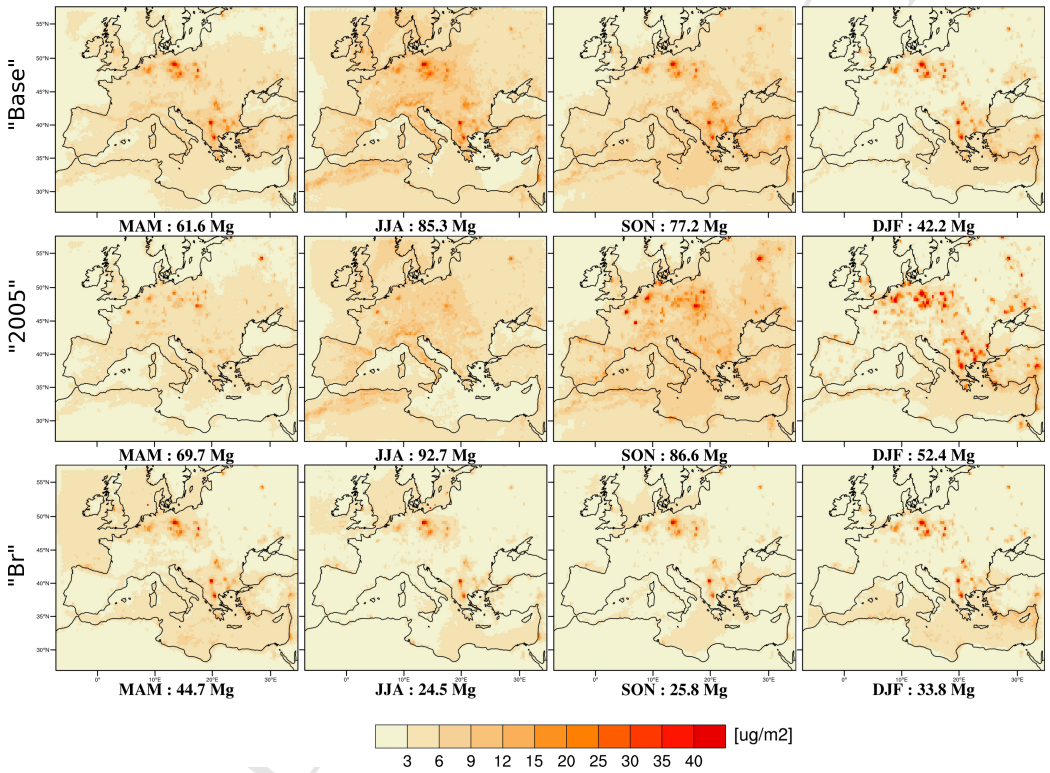

Figure 2: Seasonal total Hg deposition in the different experiments.

European and Mediterranean mercury modelling: local and long-range contributions to the deposition flux,

by,

Christian N. Gencarelli, Francesco De Simone, Ian M. Hedgecock, Francesca Sprovieri, Xin Yang and Nicola Pirrone

Highlights:

- Gas phase conversion of Hg^0 to Hg^{II} by O_3/OH is inconsistent with observations
- A Br/BrO oxidation mechanism compared best with observed Hg precipitation fluxes
- Local emissions contribute most to the overall Hg deposition flux in the summer
- Long-range transport of Hg contributes most to Europe winter Hg deposition

Supplementary Information for European and Mediterranean mercury modelling: local and long-range contributions to the deposition flux

Christian N. Gencarelli[a], Francesco De Simone[a], Ian M. Hedgecock[a], Nicola Pirrone[b], Francesca Sprovieri[a], Xin Yang[c]

[a] *CNR-Institute of Atmospheric Pollution Research, Division of Rende, Rende, Italy*
[b] *CNR-Institute of Atmospheric Pollution Research, Rome, Italy*
[c] *British Antarctic Survey,Cambridge,United Kingdom*

Appendix A. Supplementary Information

Appendix A.1. Model Set-up

Using KPP (Damian et al., 2002; Sandu et al., 2003; Sandu and Sander, 2006) and the WKC coupler (Salzmann and Lawrence, 2006) mercury species ($Hg^0Hg^PHg^{II}Hg^{II}_{aq}$) have been added to the RADM2 (Stockwell et al., 1990) chemical mechanism. Hg^0 and Hg^{II} represent Gaseaous elemental mercury and gaseous oxides mercury respectively. Hg^P represents Hg associated with particulate which is emitted from anthropogenic sources (and is considered insluble), and Hg^{II}_{aq} represents Hg which has been oxidised in the atmosphere and is considered as particulte when the atmospheric liquid water content is below a threshold value. In the presence of model cell liquid water content above the threshold value, Hg^{II}_{aq} is assumed to be completely scavenged by the aqueous phase. Dry deposition of Hg species in WRF/Chem is treated using the approach developed by Wesely (1989) and calculated as described by Lin et al. (2006), with a deposition velocity for Hg^{II} equal to that of $HNO_{3(g)}$ (due to the similarity in their solubility (Seigneur et al., 2004), while for Hg^P and $HgIHg^{II}_{aq}$, the dry deposition flux is calculated using WRF/Chem particulate deposition parametrisations. Wet deposition of Hg species has

Email address: ihedegcock@iia.cnr.it (Ian M. Hedgecock)

been implemented by adding Hg compounds to the scheme in WRF/Chem for gas and particulate convective transport and wet deposition. In-cloud and below-cloud scavenging of Hg species was included by adapting an already available module in WRF/Chem, based on the approach described by Neu and Prather (2012). In the model, the fraction of the grid box exposed to scavenging is calculated using the algorithm described in Neu and Prather (2012), and the Hg species scavenging rate is assumed to be the same as that for $HNO_{3(g)}$. For convective deposition the original WRF/Chem routine (based on the Grell and Dévényi (2002) parameterization) has been adapted to include the deposition of Hg^{II}_{aq} resulting from convective precipitation.

Dry deposition of Hg^0 and its re-emission have recently been reviewed by Zhang et al. (2009). There is still significant uncertainty associated with the net Hg^0 flux (and its direction) over terrestrial surfaces, and therefore in this version of the model, it has not been included. Moreover dry and wet deposition of $Hg^0 is assumed to be negligible in comparison Hg^P Hg^{II} and Hg^{II}_{aq}$ deposition, with a magnitude equivalent to emissions from natural sources (Baker and Bash, 2012).

Inventory (Total in Mg)	2005 (219.6)			2010 (145.9)		
Hg Species	Hg^0	Hg^{II}	Hg^P	Hg^0	Hg^{II}	Hg^P
Total (%)	60	32	8	65	28	7
0 - 50 m (%)	26	17	4	13	6	1
50 - 150 m (%)	20	4	1	30	5	2
> 150 m (%)	14	11	3	22	17	4

Table A.1: Comparison of the 2005 and 2010 AMAP/UNEP emission inventories (AMAP/UNEP, 2008, 2013), totals, specaition and height distribution.
1

	Observations	"Base"			"2005"			"Br"		
station	Mean ± SD	Mean ± SD	RMSE	bias	Mean ± SD	RMSE	bias	Mean ± SD	RMSE	bias
CZ03	0.68±0.62	1.50±0.13	1.00	0.82	1.53±0.11	1.05	0.85	1.55±0.08	1.04	0.87
DE02	1.69±0.13	1.66±0.12	0.13	-0.03	1.68±0.10	0.16	-0.01	1.69±0.09	0.11	0.00
DE08	1.70±0.17	1.52±0.12	0.25	-0.18	1.54±0.10	0.23	-0.16	1.55±0.08	0.21	-0.15
DE09	1.48±0.22	1.65±0.10	0.24	0.17	1.65±0.09	0.24	0.17	1.67±0.06	0.27	0.19
GB48	1.11±0.34	1.52±0.04	0.52	0.41	1.55±0.03	0.54	0.44	1.53±0.03	0.52	0.42
NO01	1.68±0.18	1.54±0.07	0.23	-0.14	1.55±0.07	0.23	-0.13	1.55±0.04	0.22	-0.13
PL05	1.25±0.25	1.58±0.12	0.37	0.33	1.62±0.11	0.42	0.37	1.60±0.09	0.39	0.35
SE11	1.40±0.14	1.61±0.09	0.23	0.21	1.64±0.08	0.26	0.24	1.62±0.06	0.24	0.22
SE14	1.51±0.11	1.59±0.08	0.12	0.08	1.60±0.07	0.13	0.09	1.60±0.06	0.12	0.09

Table A.2: TGM concentration statistical analysis in the EMEP stations. Mean (M), Standard Deviation (SD) and Root Mean Square Error (RMSE) and bias are in $\mathrm{ng\,m^{-3}}$.

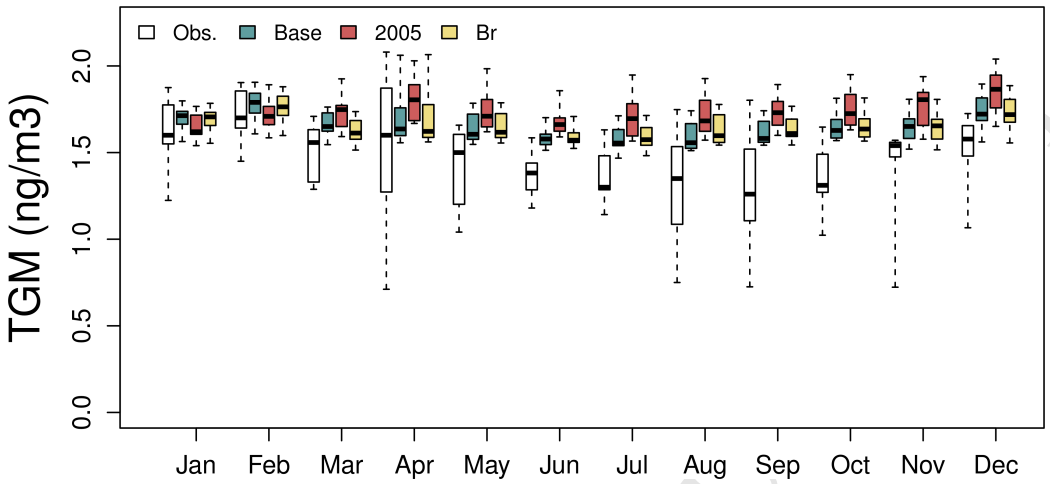

Figure A.1: Monthly distribution of measured and modelled TGM concentrations at EMEP measurement stations.

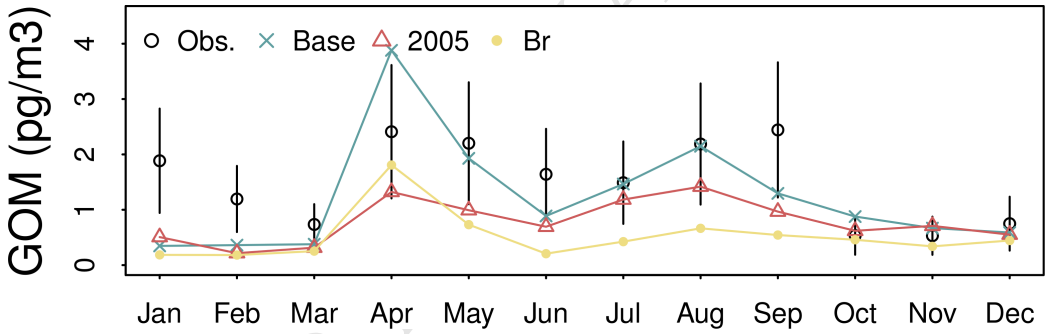

Figure A.2: Monthly distribution of measured and modelled PBM concentrations at EMEP measurement stations.

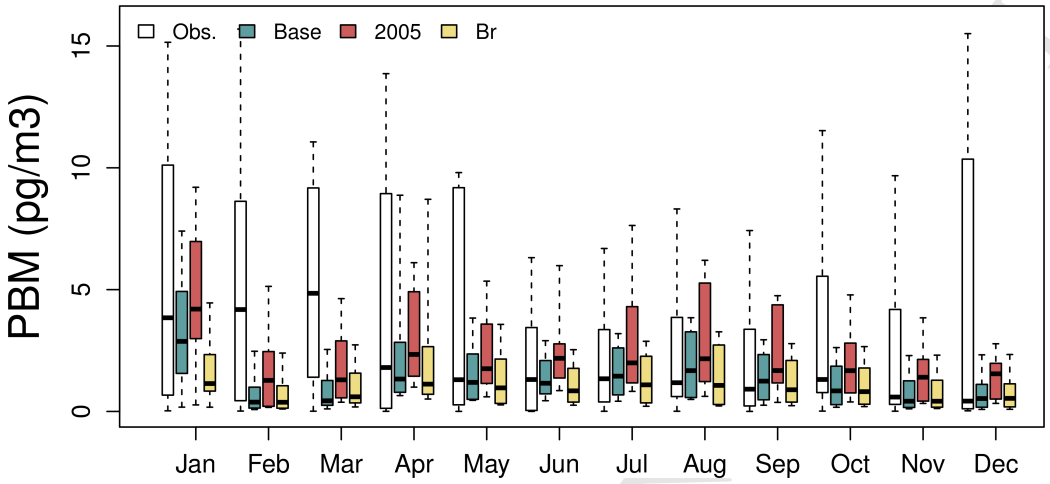

Figure A.3: Monthly distribution of measured and modelled PBM concentrations at EMEP measurement stations.

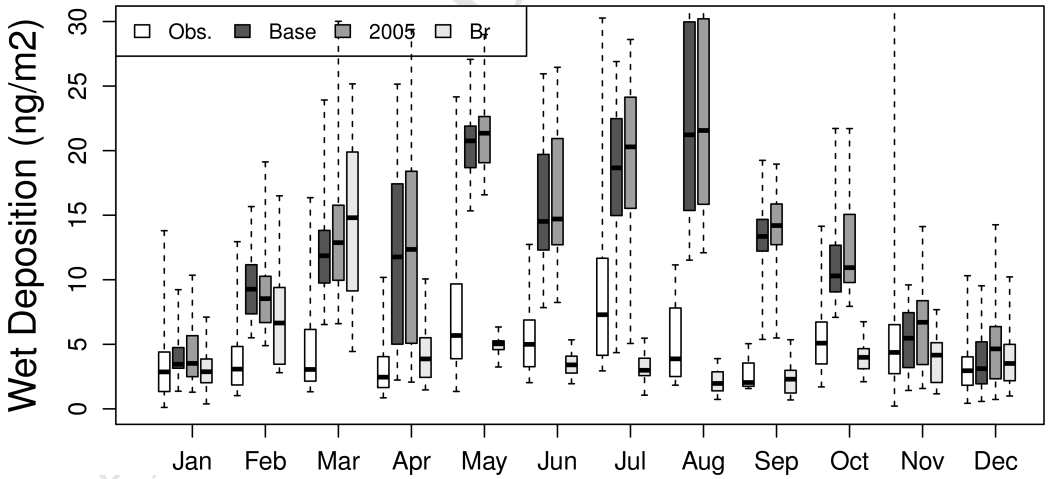

Figure A.4: Monthly mean to the mercury wet deposition flux in EMEP sites and in correspondents model cells.

	Mean Obs	Mean Model			bias			RMSE		
station		Base	2005	Br	Base	2005	Br	Base	2005	Br
BE14	9.5	31.3	30.2	10.8	21.8	20.7	1.3	31.7	30.5	9.7
DE01	7.4	16.3	15.9	9.2	8.8	8.5	1.8	13.1	12.2	8.9
DE02	8.4	29.1	28.7	11.4	20.7	20.4	3.0	24.2	23.7	7.5
DE03	10.1	17.3	15.4	4.4	7.2	5.3	-5.7	10.1	8.4	8.5
DE08	6.1	21.0	19.3	5.8	14.9	13.2	-0.4	20.7	19.0	4.9
DE09	5.7	25.3	24.9	16.7	19.6	19.2	11.0	25.0	25.1	18.6
ES08	6.8	33.9	30.3	9.6	27.1	23.5	2.8	50.1	46.1	9.3
GB13	3.8	20.3	19.8	5.2	16.6	16.0	1.5	21.1	20.5	4.0
GB17	7.0	32.1	32.3	10.7	25.2	25.3	3.8	32.4	32.0	7.7
GB48	3.5	23.4	23.1	6.2	19.9	19.6	2.7	26.4	25.8	5.6
GB91	4.6	21.0	20.9	5.5	16.5	16.3	0.9	22.8	22.4	4.9
NL91	10.1	25.6	24.9	13.7	15.6	14.8	3.7	21.3	20.4	14.2
NO01	11.1	17.8	17.1	5.6	6.8	6.1	-5.5	15.4	14.6	6.6
SE11	12.0	37.2	29.4	14.0	25.2	17.4	2.0	37.0	28.2	11.5
SE14	15.0	21.3	20.2	9.3	6.2	5.2	-5.7	11.7	9.8	8.6
SI08	5.9	16.9	16.9	4.7	11.0	11.0	-1.3	15.5	15.4	4.2

Table A.3: Comparison of the wet deposition flux statistical analysis in the EMEP stations for "Base", "2005" and "Br" simulations. The Means, Bias and Root Mean Square Error (RMSE) are in $\mathrm{ng\,m^{-2}}$.

	"Base"						"Br"					
	R_{lr}	R_{loc}	R_{lr}^{WD}	R_{loc}^{WD}	R_{lr}^{DD}	R_{loc}^{DD}	R_{lr}	R_{loc}	R_{lr}^{WD}	R_{loc}^{WD}	R_{lr}^{DD}	R_{loc}^{DD}
Jan	0.87	0.13	0.91	0.09	0.91	0.09	0.86	0.14	0.90	0.10	0.82	0.18
Feb	0.87	0.13	0.83	0.17	0.83	0.17	0.75	0.25	0.79	0.21	0.66	0.34
Mar	0.80	0.20	0.76	0.24	0.76	0.24	0.63	0.37	0.67	0.33	0.53	0.47
Apr	0.66	0.34	0.82	0.18	0.82	0.18	0.69	0.31	0.49	0.51	0.80	0.20
May	0.63	0.37	0.76	0.24	0.76	0.24	0.78	0.22	0.61	0.39	0.84	0.16
Jun	0.61	0.39	0.72	0.28	0.72	0.28	0.77	0.23	0.63	0.37	0.81	0.19
Jul	0.64	0.36	0.71	0.29	0.90	0.10	0.79	0.21	0.55	0.45	0.90	0.10
Aug	0.29	0.71	0.49	0.51	0.49	0.51	0.83	0.17	0.49	0.51	0.82	0.18
Sep	0.40	0.60	0.58	0.42	0.58	0.42	0.78	0.22	0.61	0.39	0.79	0.21
Oct	0.51	0.49	0.59	0.41	0.59	0.41	0.80	0.20	0.79	0.21	0.82	0.18
Nov	0.67	0.33	0.84	0.16	0.84	0.16	0.87	0.13	0.87	0.13	0.87	0.13
Dec	0.80	0.20	0.91	0.09	0.91	0.09	0.91	0.09	0.93	0.07	0.86	0.14

Table A.4: Pattern correlation coefficient between "Base - Local", "Base - Long-range", "Br - BrLocal" and "Br - BrLong-range", for total, only wet and only dry deposition.

References

AMAP/UNEP, 2008. Technical Background Report to the Global Atmospheric Mercury Assessment. Technical Report. Arctic Monitoring and Assessment Programme, Oslo, Norway / UNEP ChemicalsBranch, Geneva, Switzerland. URL: http://www.unep.org/hazardoussubstances/Mercury/Informationmaterials/ReportsandPublications/tabid/3593/Default.aspx.

AMAP/UNEP, 2013. Technical Background Report for the Global Mercury Assessment 2013. Technical Report. Arctic Monitoring and Assessment Programme, Oslo, Norway / UNEP ChemicalsBranch, Geneva, Switzerland. URL: http://www.unep.org/hazardoussubstances/Mercury/Informationmaterials/ReportsandPublications/tabid/3593/Default.aspx.

Baker, K.R., Bash, J.O., 2012. Regional scale photochemical model evaluation of total mercury wet deposition and speciated ambient mercury. Atmospheric Environment 49, 151–162.

Damian, V., Sandu, A., Damian, M., Potra, F., Carmichael, G., 2002. The kinetic preprocessor kpp-a software environment for solving chemical kinetics. Computers and Chemical Engineering 26, 1567–1579.

Grell, G.A., Dévényi, D., 2002. A generalized approach to parameterizing convection combining ensemble and data assimilation techniques. Geophys. Res. Lett. 29, 38–1–38–4.

Lin, C.J., Pongprueksa, P., Lindberg, S.E., Pehkonen, S.O., Byun, D., Jang, C., 2006. Scientific uncertainties in atmospheric mercury models i: Model science evaluation. Atmospheric Environment 40, 2911 – 2928.

Neu, J.L., Prather, M.J., 2012. Toward a more physical representation of precipitation scavenging in global chemistry models: cloud overlap and ice physics and their impact on tropospheric ozone. Atmospheric Chemistry and Physics 12, 3289–3310.

Salzmann, M., Lawrence, M.G., 2006. Automatic coding of chemistry solvers in WRF-Chem using KPP, in: 7th WRF Users Workshop, Boulder, Colorado, USA.

Sandu, A., Daescu, D.N., Carmichael, G.R., 2003. Direct and adjoint sensitivity analysis of chemical kinetic systems with KPP: Part I - theory and software tools. Atmospheric Environment 37, 5083 – 5096.

Sandu, A., Sander, R., 2006. Technical note: Simulating chemical systems in fortran90 and matlab with the kinetic preprocessor kpp-2.1. Atmospheric Chemistry and Physics 6, 187–195.

Seigneur, C., Vijayaraghavan, K., Lohman, K., Karamchandani, P., Scott, C., 2004. Global source attribution for mercury deposition in the united states. Environmental Science & Technology 38, 555–569.

Stockwell, W.R., Middleton, P., Chang, J.S., Taang, X., 1990. The second-generation regional acid deposition model chemical mechanism for regional air quality modelling. Journal of Geophysical Research 95, 16343–16367.

Wesely, M., 1989. Parameterization of surface resistances to gaseous dry deposition in regional-scale numerical models. Atmospheric Environment (1967) 23, 1293 – 1304.

Zhang, L., Wright, L.P., Blanchard, P., 2009. A review of current knowledge concerning dry deposition of atmospheric mercury. Atmospheric Environment 43, 5853 – 5864.

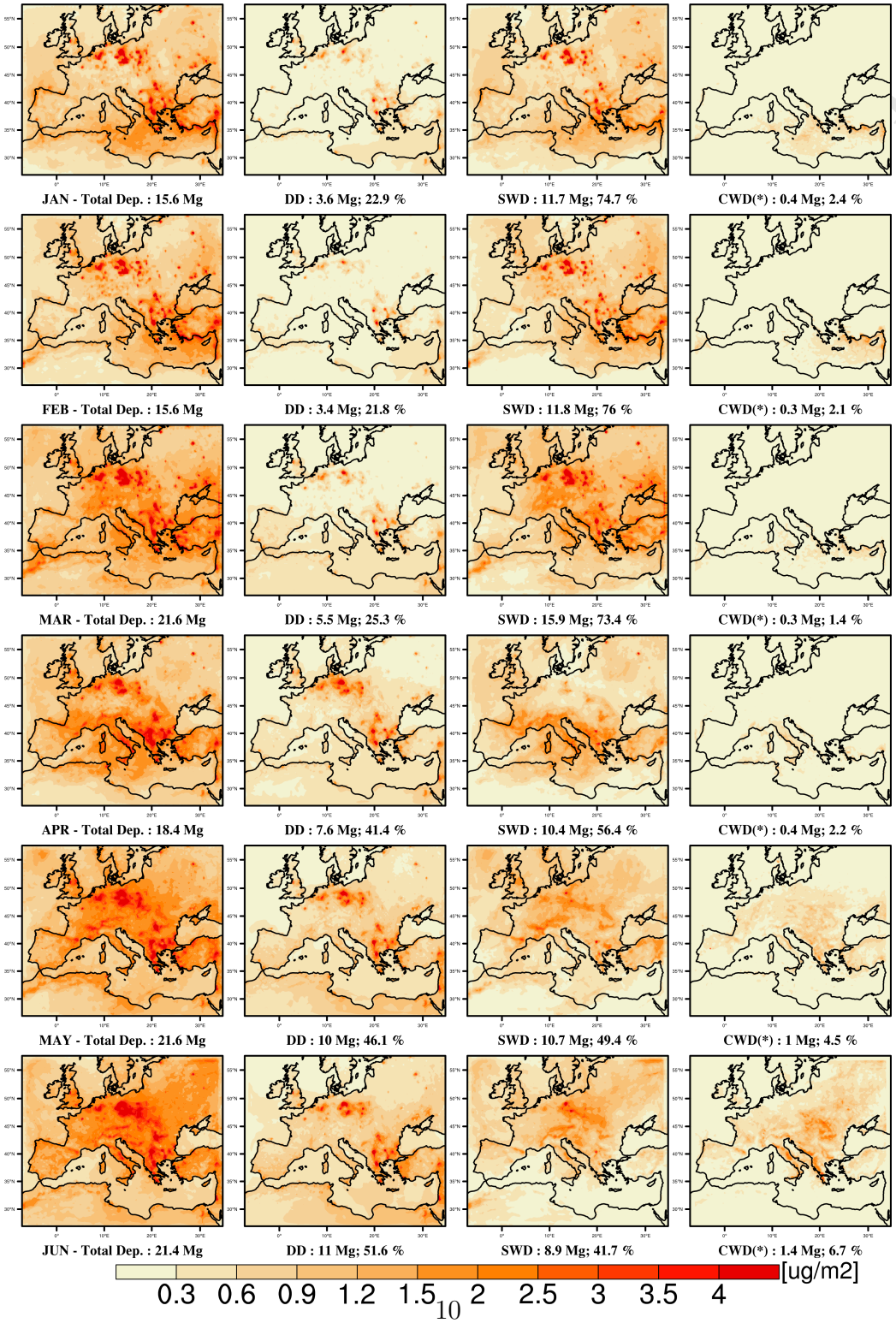

Figure A.5: Monthly total Hg deposition and fraction of DD, SWD and CWD in "Base" simulations.

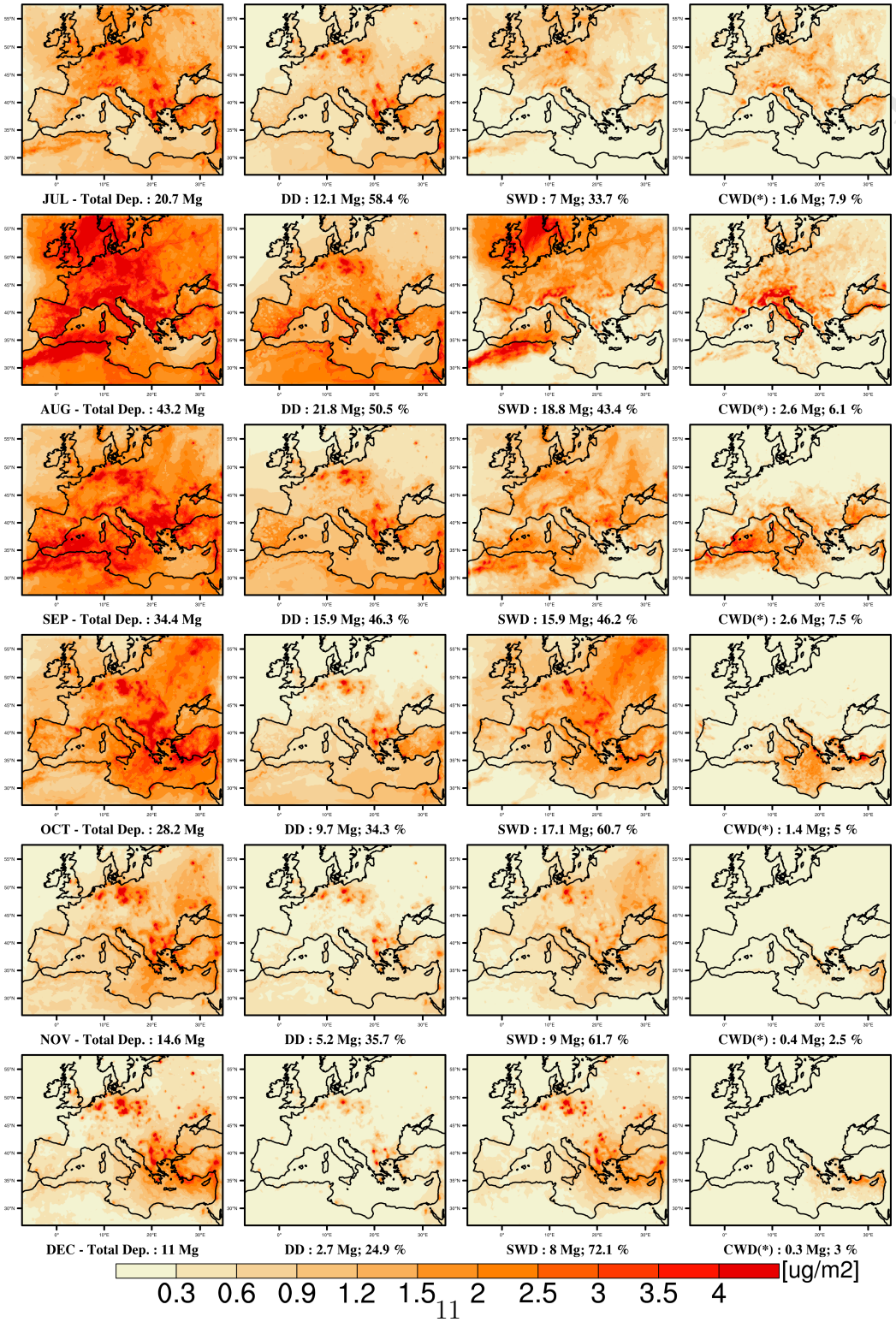

Figure A.6: Continue from figure A.5.

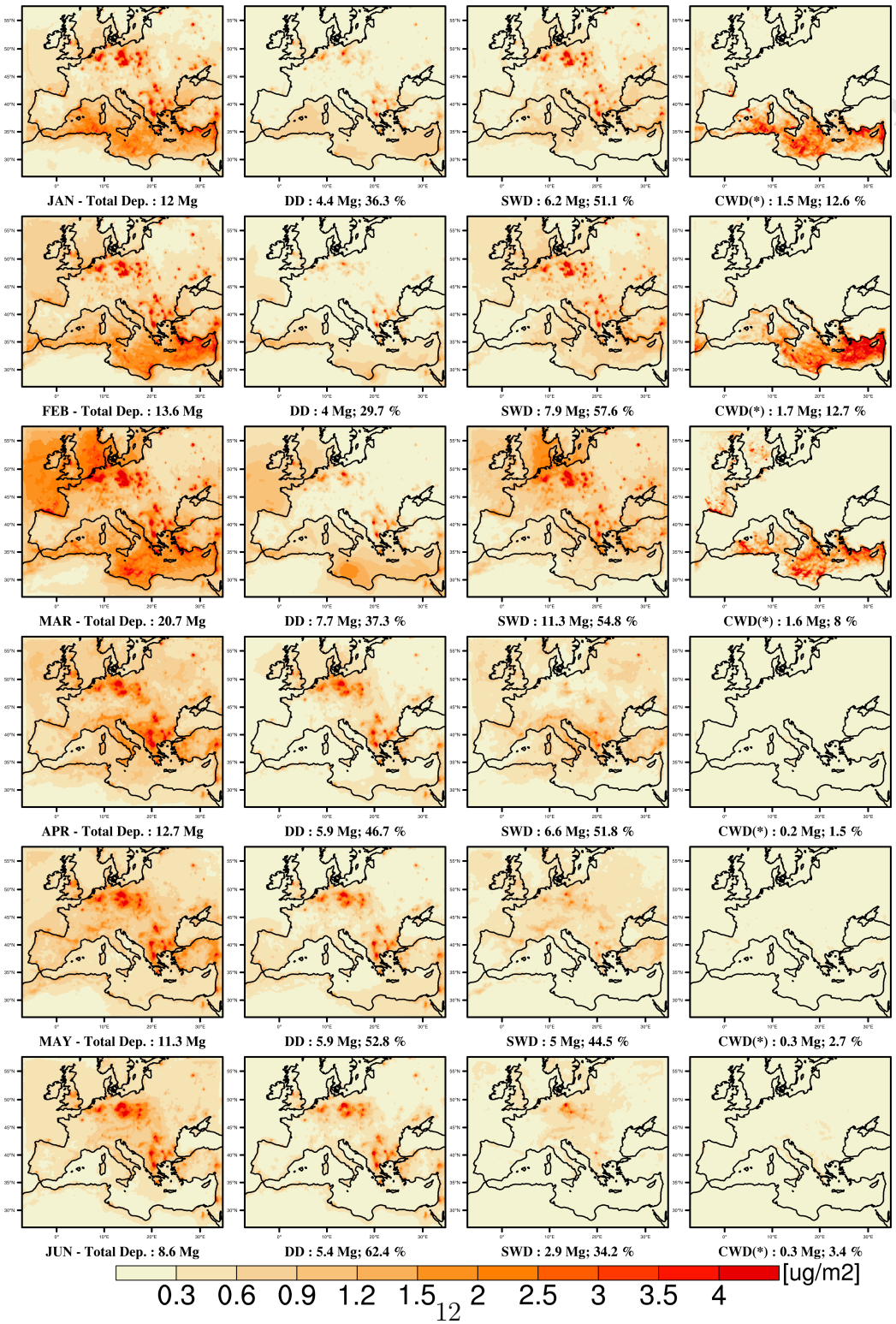

Figure A.7: Monthly total Hg deposition and fraction of DD, SWD and CWD in "Br" simulations.

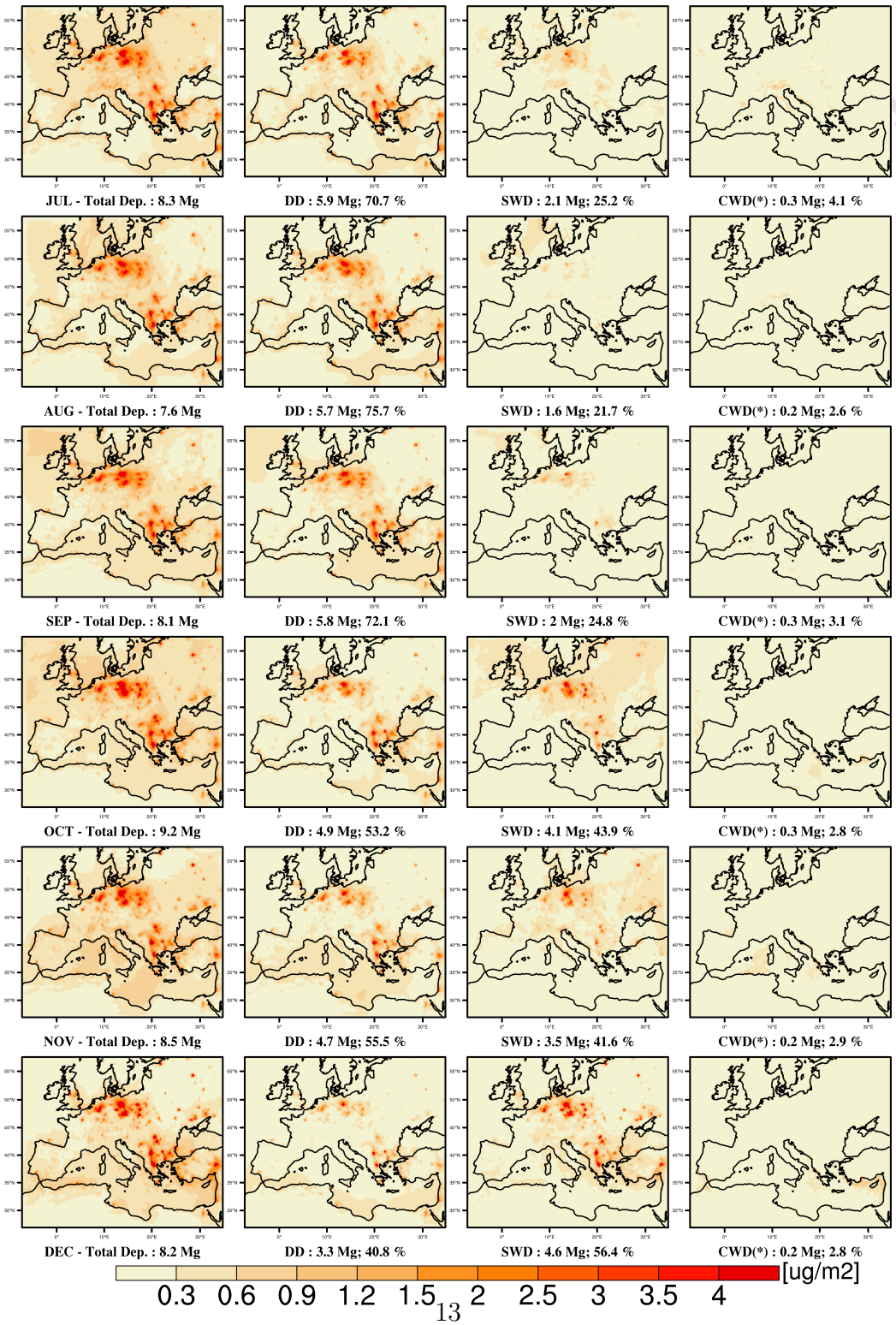

Figure A.8: Continue from figure A.7.

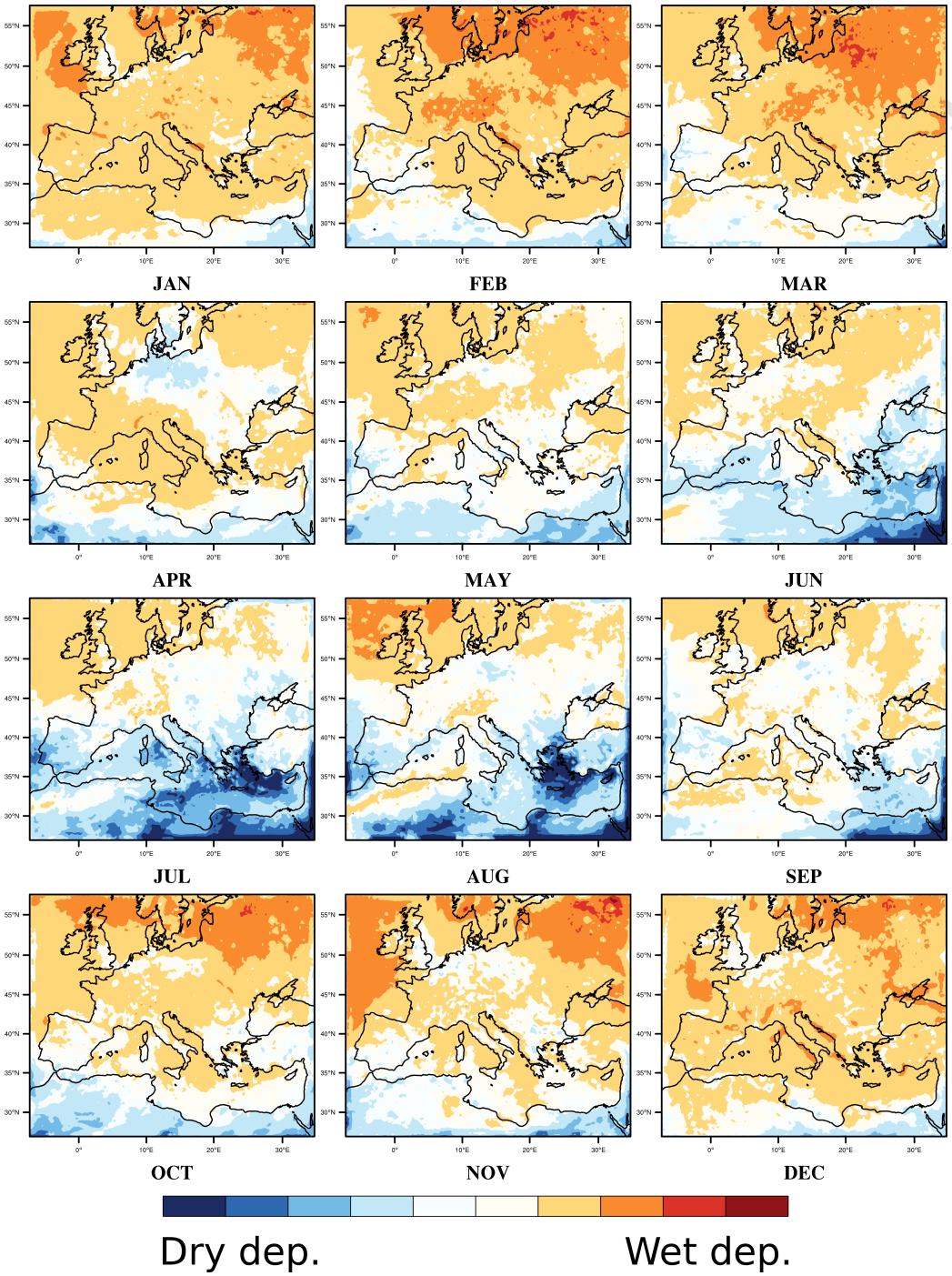

Figure A.9: Ratio between wet and dry deposition processes.